Atmospheres of polygons and knotted polygons

2008 J. Phys. A: Math. Theor. 41 105002

(http://iopscience.iop.org/1751-8121/41/10/105002)

IOP PUBLISHING JOURNAL OF PHYSICS A: MATHEMATICAL AND THEORETICAL

J. Phys. A: Math. Theor. **41** (2008) 105002 (23pp) doi:10.1088/1751-8113/41/10/105002

Atmospheres of polygons and knotted polygons

E J Janse van Rensburg[1] **and A Rechnitzer**[2]

[1] Department of Mathematics and Statistics, York University, 4700 Keele Street, Toronto, Ontario, M3J 1P3, Canada
[2] Department of Mathematics, The University of British Columbia, Vancouver, BC V6T 1Z2, Canada

E-mail: rensburg@yorku.ca and andrewr@math.ubc.ca

Received 12 December 2007, in final form 30 January 2008
Published 26 February 2008
Online at stacks.iop.org/JPhysA/41/105002

Abstract

In this paper we define two statistics $a_+(\omega)$ and $a_-(\omega)$, the *positive* and *negative* atmospheres of a lattice polygon ω of fixed length n. These statistics have the property that $\langle a_+(\omega)\rangle/\langle a_-(\omega)\rangle = p_{n+2}/p_n$, where p_n is the number of polygons of length n, counted modulo translations. We use the pivot algorithm to sample polygons and to compute the corresponding average atmospheres. Using these data, we directly estimate the growth constants of polygons in two and three dimensions. We find that

$$\mu = \begin{cases} 2.638\,05 \pm 0.000\,12, & \text{in two dimensions;} \\ 4.683\,980 \pm 0.000\,042 \pm 0.000\,067, & \text{in three dimensions,} \end{cases}$$

where the error bars are 67% confidence intervals, and the second error bar in the three-dimensional estimate of μ is an estimated systematic error. We also compute atmospheres of polygons of fixed knot type K sampled by the BFACF algorithm. We discuss the implications of our results and show that different knot types have atmospheres which behave dramatically differently at small values of n.

PACS numbers: 02.10.Kn, 36.20.Ey, 05.70.Jk, 87.15.Aa

1. Introduction

Lattice polygons are models of ring polymers with excluded volume and remain a mathematically rich and unsolved model in statistical mechanics [6, 9, 10]. This model poses a basic combinatorial question, namely, how many distinct polygons of length n are there in the hypercubic lattice [15]? This question is related to the combinatorics of self-avoiding walks. If c_n is the number of self-avoiding walks from the origin, of length n, then it is known that the limit

$$\mu = \lim_{n\to\infty} c_n^{1/n} \tag{1}$$

exists in d dimensions and $\mu > 1$ in dimensions $d > 1$ [16]. The constant μ is the *growth constant* of the self-avoiding walk, while $\kappa = \log \mu$ is the *connective constant* [4]. Several basic properties of c_n are known; for example, it is known that the limit

$$\mu^2 = \lim_{n\to\infty} c_{n+2}/c_n \tag{2}$$

exists [27, 28], but the stronger result $\mu = \lim_{n\to\infty} c_{n+1}/c_n$ remains unproven in the square or cubic lattice [14] (but is known for non-bipartite lattices such as the triangular lattice [32]). It has been also established that $c_{n+1} > c_n$ [38] in general. There are overwhelming numerical and other evidence that

$$c_n = A\mu^n n^{\gamma-1}\,(1 + o(1))\,, \tag{3}$$

where γ is referred to as the *entropic exponent* of the self-avoiding walk.

A lattice polygon is an unrooted embedding of the unlabelled cycle graph in the hypercubic lattice. The length of a lattice polygon is the number of lattice edges its contains. Lattice polygons have been the subject of much attention over the last 50 years. If p_n is the number of polygons of length n in the hypercubic lattice (counted up to translational invariance), then the limit

$$\mu = \lim_{n\to\infty} p_n^{1/n} \tag{4}$$

is known to exist [15], and the growth constant of polygons is equal in numerical value to the growth constant of self-avoiding walks defined in equation (1). It is widely accepted that the asymptotic growth of p_n is of the form

$$p_n = An^{\alpha-2}\mu^n(1 + o(1)), \tag{5}$$

where α is the *polygon entropic exponent* or the *specific heat exponent*. The function p_n satisfies

$$\lim_{n\to\infty} \frac{p_{n+2}}{p_n} = \mu^2, \tag{6}$$

a result due to Kesten [27, 28] (see [32] for a simpler proof).

The numerical value of μ has been estimated in the square lattice using a variety of different methods, including computer enumeration and series analysis of lattice polygons and self-avoiding walks, or grand canonical Monte Carlo simulations (in such simulations polygons are sampled from a Boltzman distribution over the lengths of the polygons or walks). The best estimates for μ have been obtained from computer enumeration and series analysis.

Series analysis for polygons [25, 26] gives μ and α to very high precision[3]:

$$\mu = 2.638\,158\,530\,34 \pm 0.000\,000\,000\,10, \tag{7}$$

$$\alpha = 0.500\,0005 \pm 0.000\,0010. \tag{8}$$

See also [23] for a slight improvement on these values. The exponent α has also been estimated from conformal field theory and Coulomb gas methods, which gives the exact value $\alpha = 1/2$ in two dimensions [35, 36].

Determining μ from self-avoiding walk data is not so successful. The best estimate for μ and the entropic exponent γ in equation (3) obtained from self-avoiding walk data are

$$\mu = 2.638\,158\,56 \pm 0.000\,000\,03, \tag{9}$$

$$\gamma = 1.343\,745 \pm 0.000\,015, \tag{10}$$

as determined in [24], see [13] for additional results.

[3] Error bars and confidence intervals are those claimed in the original references. In this paper, we state our own error bars as 67% statistical confidence intervals.

Less precise estimates for μ and α are available in three dimensions. Clisby, Liang and Slade [5] estimated that

$$\mu = 4.684\,044 \pm 0.000\,011, \tag{11}$$

$$\alpha \approx 0.24 \tag{12}$$

by collecting series data on the self-avoiding walk using the lace expansion. The exponent α has also been determined by field theoretic means [12, 29], giving $\alpha = 0.237 \pm 0.002$. This exponent has also been computed to higher precision by first computing the metric exponent ν of polygons, and then by using the hyperscaling relation $\mathrm{d}\nu = 2 - \alpha$. However, independent estimates of α should be made to test the validity of this relation.

In [43] a new statistic called the *atmosphere* of a self-avoiding walk was introduced. This statistic was shown (numerically) to converge to the growth constant μ as the length of the walk increases, and it is possible to determine estimates of μ and γ using canonical Monte Carlo simulation (of fixed length self-avoiding walks) [31].

We define the atmosphere of an (oriented) self-avoiding walk as the set of edges which may be appended onto its last vertex to extend the walk by one step while maintaining self-avoidance. Denote the size of the atmosphere of a walk w by $a(w)$. Then the mean atmosphere of walks of length n is given by

$$\langle a(w)\rangle_n = c_{n+1}/c_n. \tag{13}$$

We shall often abuse our notation by using the term 'atmosphere' to refer to both the atmosphere of the walk, and to the cardinality of the set of atmospheric edges. Equation (3) suggests that $\langle a(w)\rangle_n$ can be interpreted as a '*local estimate*' of μ. Assuming that c_n has an asymptotic form given by equation (3), then

$$\langle a\rangle_n = \mu\left(1 + \frac{\gamma - 1}{n} + o(1/n)\right). \tag{14}$$

Consequently, by obtaining precise estimates of the mean atmosphere of self-avoiding walks at various *fixed* lengths, estimates of both μ and γ were obtained

$$\mu = 2.638\,16 \pm 0.000\,06, \qquad \gamma = 1.345 \pm 0.002. \tag{15}$$

These results verify digits obtained by computer and series enumeration [13] above in equation (9).

Previously, Monte Carlo estimates for μ and γ have been made using grand canonical Monte Carlo algorithms which samples self-avoiding walks from a distribution over their lengths. The most well-known such algorithm is the Beretti–Sokal algorithm [3]. This algorithm has produced estimates of the connective constant as follows [37]:

$$\mu = 2.638\,164 \pm 0.000\,014, \tag{16}$$

with error bars a combined 95% statistical confidence interval and an estimated systematic error due to uncertainties in the model. More recently the [11, 42] PERM algorithm has been used to find precise estimates of μ and γ in three dimensions and higher.

In section 2 of this paper, we define a new statistic for polygons which plays the same role as the atmosphere statistic in walks. We show that the mean *atmospheres* of a polygon can be used to estimate μ and α in equation (5). Data were collected for polygons on the square and cubic lattices in two and in three dimensions, and by analysing the data (see section 3), we estimate that

$$\mu = 2.638\,05 \pm 0.000\,12, \qquad \alpha = 0.532 \pm 0.027 \tag{17}$$

in two dimensions, and

$$\begin{aligned}\mu &= 4.683\,980 \pm 0.000\,042 \pm 0.000\,067,\\ \alpha &= 0.248 \pm 0.016\end{aligned} \tag{18}$$

in three dimensions. The statistical error bars are 67% statistical confidence intervals, and the second error bar in the three-dimensional estimate of μ is an estimated systematic error.

The estimate in three dimensions compare well to estimates in the literature. For example, [17] reported an (unpublished) estimate $\mu = 4.683\,907 \pm 0.000\,022$ due to A J Guttmann, while the best published estimate is due to self-avoiding walk enumeration using the lace expansion [5]. This gives $\mu = 4.684\,043 \pm 0.000\,012$. The estimates in equation (18) above were obtained using relatively modest computer resources, and are consistent with those in [5].

In section 4, we shift our attention to knotted polygons. The atmospheric statistic can be used to make numerical estimates of the ratios $p_{n+2}(K)/p_n(K)$ of the number of polygons of length $n+2$ and length n, and of knot type K. If the entropy of a polygon of length n is defined by $\log p_n(K)$, then the logarithm of the ratio $p_{n+2}(K)/p_n(K)$ is the relative entropy of the polygon, and is a measure of the change in entropy with increasing n. For example, in figure 8 we plot numerical estimates of the ratio $p_{n+2}(\emptyset)/p_n(\emptyset)$ for unknotted polygons. The data increase at small n and quickly settles down to a constant. The increase at small n implies that the rate of increase in $\log p_n(\emptyset)$ increases at small n. This is in contrast with polygons of fixed non-trivial knot type, as illustrated in for example in figure 9 for trefoils. The rate of increase in $\log p_n(3_1)$ decreases with increasing n at small values of n before settling down to a constant within numerical variation. These data also indicate that the growth constant of a knotted polygon of fixed knot type is independent of knot type, but that the approach of $[p_n(K)]^{1/n}$ to μ_K is from below for unknots, and from above for knotted polygons of fixed non-trivial knot type. We make some final comments in section 5, and in the appendix we show how the atmosphere statistic can be generalized to interacting models of polygons. This technique gives a method for directly estimating the limiting free energy of an interacting polygon.

2. Atmospheres of polygons

Let ω be a polygon, and let e be an edge in the polygon. Incident with e are $2(d-1)$ unit squares in the d-dimensional hypercubic lattice. Each of these unit squares S has at least one edge (e) in ω. We say that S is part of the *positive atmosphere* of ω if it has exactly one edge (e) in ω and is otherwise disjoint with ω. In this event, one may change ω so that it traverses the *other* three edges in the boundary of S (see figure 1). Since these edges are disjoint with ω, a new self-avoiding polygon is obtained, which has length increased by two.

It is also possible that a unit square S incident with ω has exactly three boundary edges in ω. These three boundary edges form a three step walk in a $\sqcup$-conformation. If e is the middle of the edges in this three step walk, then we say S is a *negative atmospheric square* of ω incident with e. The collection of all such negative atmospheric squares incident with ω forms the *negative atmosphere* of ω. The positive and negative atmospheres of a polygon are illustrated in figure 2.

The action of adding edges to a polygon at a positive atmospheric square, or deleting edges at a negative atmospheric square, sets up a correspondence between polygons of length n and of length $n+2$. Observe that the addition of two edges at a positive atmospheric square as in figure 1 changes that positive atmospheric square into a negative atmospheric square.

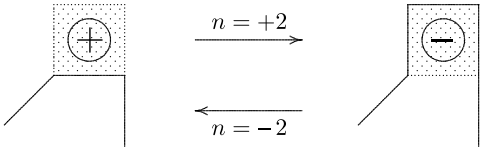

Figure 1. The atmosphere of a polygon: by adding two edges to the polygon around the square on the left, a polygon is found which has length increased by two. The collection of such squares incident with a polygon is its *positive atmosphere*. On the other hand, by instead deleting two edges to remove the square, we obtain a polygon which has length reduced by two. The collection of such squares incident with a polygon is its *negative atmosphere*.

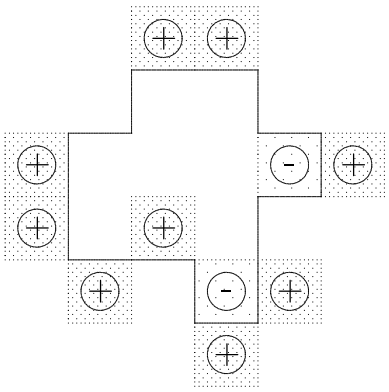

Figure 2. The atmosphere of a two-dimensional polygon. The positive atmosphere is composed of the darker shaded unit squares. The negative atmosphere is composed of the lighter shaded unit squares. By adding two edges in the polygon so that it includes three edges of a positive atmosphere square, a new polygon is obtained which includes the atmospheric square as part of its negative atmosphere. By removing two edges from the polygon so that a negative atmospheric square is removed, a new polygon is obtained which includes the atmospheric square as part of its positive atmosphere.

Similarly, if edges are deleted to cut a negative atmospheric square from a polygon as in figure 1, then that negative atmospheric square is changed into a positive atmospheric square.

To examine this correspondence between negative and positive atmospheres, define $p_n(a_+, a_-)$ to be the number of lattice polygons of length n with a_+ positive atmospheric squares, and a_- negative atmospheric squares. Observe that each polygon has at least two positive atmospheric squares located on the edges with lexicographic most and least midpoints. There are some polygons with zero negative atmospheric squares, for example, any polygon that is a geometric rectangle with sides longer than 2 in lengths has no negative atmospheric squares.

The total number of ways that we can extend the length of a polygon by two edges in this way is $\sum_{a_+,a_-} a_+ p_n(a_+, a_-)$, and the result is in each case a polygon of length $n + 2$. Each polygon of length $n + 2$ obtained in this way has at least one negative atmospheric square, and is the image of exactly a_- polygons if it has a_- negative atmospheric squares. In other words, each polygon of length $n + 2$ with a_- negative atmospheric squares are counted a_- times by the sum $\sum_{a_+,a_-} a_+ p_n(a_+, a_-)$. Hence

$$\sum_{a_+,a_-} a_+ p_n(a_+, a_-) = \sum_{a_+,a_-} a_- p_{n+2}(a_+, a_-), \tag{19}$$

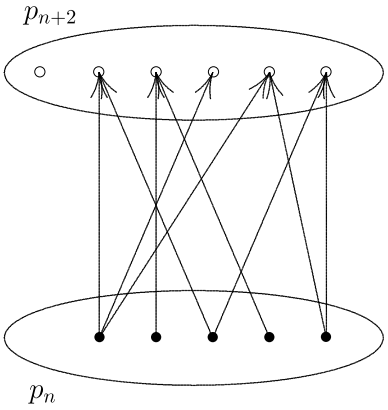

Figure 3. Polygons of length n can be mapped to polygons of length p_{n+2} by adding edges around an atmospheric square. In this schematic diagram, polygons of length n are mapped to polygons of length $n+2$ along the arrows. Observe that each arrow corresponds to a positive atmospheric square on a polygon counted by p_n, or to a negative atmospheric square on a polygon counted by p_{n+2}. Each polygon of length n may be mapped to a number of different polygons of length $n+2$ by adding the edges round a positive atmospheric square. The total number of arrows is equal to the number of ways edges can be added around positive atmospheric squares on polygons of length n. Conversely, by removing edges from a negative atmospheric square in a polygon of length $n+2$, a polygon of length $n+2$ is mapped to a polygon of length n. In the diagram above, moving against each arrow corresponds to the removal of edges from a negative atmospheric square. There may be some polygons of length $n+2$ without negative atmospheres. It follows that the number of arrows can be counted by either considering the addition of edges around positive atmospheric squares on polygons of length n, or by considering the removal of edges around negative atmospheric squares. This observation gives equation (23).

where both sums are over all values of $a_+ \geqslant 0$ and $a_- \geqslant 0$ since $\sum_{a_+,a_-} p_n(a_+, a_-) = p_n$. Observe that the sums in equation (19) give the number of arrows in figure 3; in the first case these are counted from the positive atmospheres of polygons of length n and in the second case from the negative atmospheres of polygons of length $n+2$.

We proceed by defining the mean positive atmosphere of a polygon of length n by

$$\langle a_+ \rangle_n = \frac{\sum_{a_+,a_-} a_+ p_n(a_+, a_-)}{p_n} \tag{20}$$

and the mean negative atmosphere of the polygon of length n by

$$\langle a_- \rangle_n = \frac{\sum_{a_+,a_-} a_- p_n(a_+, a_-)}{p_n}. \tag{21}$$

Comparison of this with equation (19) shows that

$$\langle a_+ \rangle_n = \langle a_- \rangle_{n+2} \frac{p_{n+2}}{p_n}. \tag{22}$$

This may be rearranged to

$$\frac{p_{n+2}}{p_n} = \frac{\langle a_+ \rangle_n}{\langle a_- \rangle_{n+2}}. \tag{23}$$

As $n \to \infty$ this converges to μ^2 (see equation (6). Hence, estimating the ratio of atmospheres on the right-hand side for a range of values of n, and then extrapolating in n, will give an estimate of μ^2.

Define the average positive atmosphere per edge by $\langle a_+/n \rangle_n$ (and similarly for $\langle a_-/n \rangle_n$). Kesten's pattern theorem [27, 28] shows that both $\langle a_+/n \rangle_n$ and $\langle a_-/n \rangle_n$ are bounded as

Table 1. Polygon atmospheres in two dimensions. The estimates for $\langle a_+/a_-\rangle_n$ are modified by putting $a_- = 1$ whenever the negative atmosphere of a polygon is empty. In addition, observe that these raw data give two times $\langle a_+\rangle_n$ and $\langle a_-\rangle_n$.

n	$\langle a_+/a_-\rangle_n$	$2\langle a_+\rangle_n$	$2\langle a_-\rangle_n$	Ratio
10	5.3623 ± 0.0098	15.7175 ± 0.0145	3.4264 ± 0.0064	4.587 ± 0.013
16	7.374 ± 0.017	23.257 ± 0.023	4.1136 ± 0.0076	5.5668 ± 0.0179
20	8.095 ± 0.022	28.905 ± 0.031	4.8489 ± 0.0098	5.961 ± 0.019
30	8.654 ± 0.029	43.513 ± 0.050	6.9189 ± 0.0142	6.289 ± 0.021
40	8.449 ± 0.026	58.459 ± 0.051	9.0830 ± 0.0156	6.4361 ± 0.0167
50	8.173 ± 0.023	73.544 ± 0.055	11.2410 ± 0.0177	6.5425 ± 0.0152
60	7.932 ± 0.021	88.713 ± 0.064	13.4015 ± 0.0198	6.6196 ± 0.0146
80	7.6280 ± 0.0153	119.014 ± 0.071	17.725 ± 0.022	6.7145 ± 0.0124
100	7.4566 ± 0.0132	149.376 ± 0.078	22.094 ± 0.025	6.7609 ± 0.0112
120	7.3372 ± 0.0116	179.590 ± 0.091	26.494 ± 0.028	6.7785 ± 0.0106
150	7.2690 ± 0.0099	225.207 ± 0.099	32.940 ± 0.031	6.8369 ± 0.0095
200	7.1776 ± 0.0091	300.817 ± 0.121	43.887 ± 0.037	6.8544 ± 0.0086
250	7.1152 ± 0.0080	376.339 ± 0.140	54.834 ± 0.042	6.8632 ± 0.0079
300	7.1047 ± 0.0068	452.416 ± 0.147	65.627 ± 0.044	6.8937 ± 0.0069
350	7.0935 ± 0.0067	528.410 ± 0.167	76.401 ± 0.051	6.9163 ± 0.0069
400	7.0598 ± 0.0061	603.730 ± 0.177	87.424 ± 0.053	6.9058 ± 0.0063
500	7.0458 ± 0.0056	755.49 ± 0.21	109.128 ± 0.063	6.9230 ± 0.0060
600	7.0334 ± 0.0052	907.12 ± 0.23	130.852 ± 0.068	6.9324 ± 0.0054
700	7.0082 ± 0.0049	1057.95 ± 0.25	152.839 ± 0.077	6.9220 ± 0.0052
800	7.0103 ± 0.0046	1209.63 ± 0.27	174.445 ± 0.083	6.9342 ± 0.0049
900	7.0039 ± 0.0045	1361.13 ± 0.30	196.200 ± 0.093	6.9375 ± 0.0049
1000	6.9970 ± 0.0034	1512.48 ± 0.25	218.150 ± 0.076	6.9332 ± 0.0036
1200	6.9877 ± 0.0032	1815.37 ± 0.29	261.681 ± 0.086	6.9373 ± 0.0034
1500	6.9822 ± 0.0030	2269.94 ± 0.33	326.991 ± 0.099	6.9419 ± 0.0032
2000	6.9794 ± 0.0026	3027.62 ± 0.38	435.611 ± 0.118	6.9503 ± 0.0028
2500	6.9761 ± 0.0021	3784.80 ± 0.39	544.403 ± 0.117	6.9522 ± 0.0022
3000	6.97005 ± 0.00194	4541.54 ± 0.43	653.443 ± 0.132	6.9502 ± 0.0021
3500	6.97188 ± 0.00181	5299.21 ± 0.47	761.955 ± 0.146	6.9548 ± 0.0020
4000	6.96912 ± 0.00168	6056.95 ± 0.51	870.833 ± 0.153	6.9554 ± 0.0019
5000	6.96873 ± 0.00157	7571.18 ± 0.59	1088.313 ± 0.179	6.9568 ± 0.0017

$n \to \infty$. If one assumes that these averages approach constants as $n \to \infty$, then equation (23) may be approximated by

$$\frac{p_{n+2}}{p_n} \approx \frac{\langle a_+/n\rangle_n}{\langle a_-/n\rangle_n}, \tag{24}$$

where the right-hand side converges to a constant as $n \to \infty$ in which case the approximation becomes exact.

The averages $\langle a_\pm/n\rangle = \langle a_\pm\rangle/n$ can be collected using the pivot algorithm for polygons at fixed values of n [30]. Since each atmosphere is computed by examining each edge of a polygon, it follows that atmospheres are typically $O(nd)$ in a d-dimensional polygon of length n. In contrast, the atmospheres defined for the self-avoiding walk in [20, 43] are $O(d)$.

3. Connective constants of polygons on the square and cubic lattice

The pivot algorithm for polygons [22, 30] was used to collect atmospheric data in two dimensions (see table 1) and in three dimensions (see table 4). The lengths of polygons

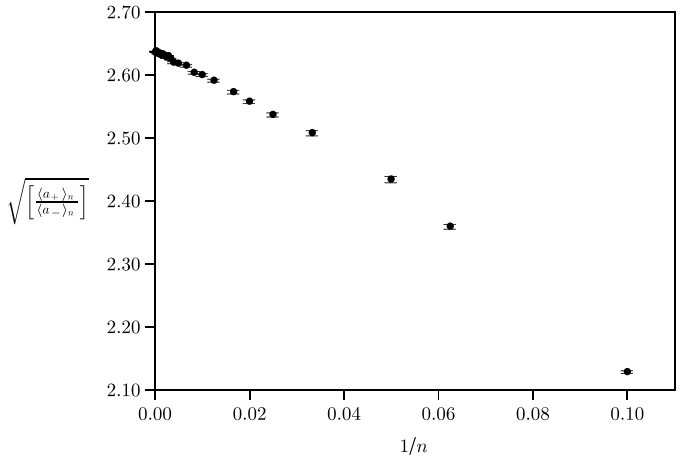

Figure 4. The ratio $[\langle a_+\rangle_n/\langle a_-\rangle_n]^{1/2}$ plotted against $1/n$ in the square lattice. Extrapolation of the data to infinite n is done by a regression with the model $2d-1$ to estimate μ.

was set at values between 10 and 5000, and for each value of n (except $n = 700$ and $n = 5000$, where we did more iterations), the number of iterations (an iteration is an attempted pivot move) was set at $N \times 10^5 n$ with data collected every $\lceil n/10 \rceil$ iterations. This produced a time series of length $10^6 N$, which we analysed to compute averages. Autocorrelation times along the time series were computed using a windowing scheme (see [31]) and were found to be of lengths less than 40 along the time series in the worst cases. The values of N used were $N = 2$ for $n < 1000$, $N = 3$ for $1000 \leqslant n < 2500$ and $N = 4$ for $2500 \leqslant n \leqslant 5000$. To reduce initialization bias in our data, we discarded the first n^2 attempted pivots in each run. For example, for $n = 1000$ we discarded the first 10^6 iterations. Our simulations took some weeks of CPU time on desktop workstations.

3.1. Results in two dimensions

Data collected in two dimensions are tabulated in table 1. The ratios of the atmospheres were also collected, and these are plotted in figure 4 against $1/n$. It appears that the ratio of the atmospheres quickly approaches μ^2 with increasing n.

The data in table 1 were analysed using weighted least squares. Assuming that $p_n = An^{\alpha-2}\mu^n(1 + o(1))$ suggests fitting the data to the model

$$\frac{\langle a_+\rangle_n}{\langle a_-\rangle_n} = \mu^2 \left((n+2)/n\right)^{a_2}, \tag{25}$$

where a_2 is a constant. One would expect that $a_2 = \alpha - 2$. This model requires a nonlinear least-squares analysis and did not behave well numerically.

Instead, we took logarithms on both sides of the last equation to get the model

$$\log\left(\frac{\langle a_+\rangle_n}{\langle a_-\rangle_n}\right) = \log\mu^2 + a_2 \log\left((n+2)/n\right) + a_3/n^2, \qquad (\text{model } 2d-1), \tag{26}$$

where one extra parameter a_3 was inserted to control for deviations in the data for small values of n. Observe that $\log((n+2)/n) = 2/n + O(1/n^2)$ so that this is a linear model in $1/n$.

Linear least-squares analysis of the data in table 1 using model $2d-1$ (equation (26)) gave acceptable fits: we tracked the weighted least-square error $\chi^2(n_{\min})$ as a function of the smallest value of n ($n_{\min}$) included in the analysis. This statistic is distributed as a χ^2-statistic

Table 2. Least-squares analysis results: model $2d-1$.

$n_{\min}$	$\log \mu^2$	a_2	$\chi^2(\mathrm{d}\, f)$	Level
10	$1.939\,885 \pm 0.000\,078$	-1.314 ± 0.019	68.0(26)	100%
16	$1.940\,070 \pm 0.000\,081$	-1.451 ± 0.025	28.3(25)	70.6%
20	$1.940\,081 \pm 0.000\,083$	-1.460 ± 0.029	28.1(24)	74.4%
30	$1.940\,092 \pm 0.000\,087$	-1.470 ± 0.036	28.1(23)	78.5%
40	$1.940\,065 \pm 0.000\,090$	-1.444 ± 0.043	27.4(22)	80.2%
50	$1.940\,078 \pm 0.000\,093$	-1.458 ± 0.049	27.2(21)	83.6%

on $\mathrm{d}f$ degrees of freedom, where $\mathrm{d}f$ is the number of data-points minus the number of parameters in the model. A fit is statistically acceptable if the least-square error is acceptable at the 95% level.

The results of the analysis are given in table 2. For $n_{\min} = 16$ the fit is acceptable at the 70.6% level. In this case $\log \mu^2 = 1.940\,070 \pm 0.000\,081$ (67% statistical confidence interval). Increasing $n_{\min}$ first to 20 and then in steps to $n_{\min} = 50$ gave similar fits. For $n_{\min} > 10$ all the regressions gave a value of $\log \mu^2$ within the statistical confidence interval of the regression at $n_{\min} = 16$, and the value of $\log \mu^2$ for larger values of $n_{\min}$ settled down to a stable value within the confidence interval of its value at $n_{\min} = 16$. We took the result at $n_{\min} = 16$ as our best estimate for μ; dividing by 2 and exponentiating gives

$$\mu = 2.638\,04 \pm 0.000\,11, \tag{27}$$

with a 67% statistical confidence interval.

The value of the parameter a_2 in model (26) is consistently in the vicinity of -1.5; this agrees with the expectation that $a_2 = \alpha - 2 = -3/2$. With increasing $n_{\min}$ the estimate settles on a value that includes $-3/2$ well inside its confidence interval.

Estimates of the ratio a_+/a_- were also collected in our simulations. Since this ratio is undefined if $a_- = 0$, we modified a_- by putting $a_- = 1$ whenever the negative atmosphere of a polygon is zero. Since the probability that a polygon will have no negative atmospheric squares goes to zero quickly with increasing n, this slight modification is only relevant at small values of n, and consequently did not disturb the average at higher values of n. Our estimates are also listed in table 1. These data were similarly analysed using the three parameter model

$$\log \left\langle \frac{a_+}{a_-} \right\rangle_n = \log \mu^2 + a_2 \log((n+2)/n)) + a_3/n^2, \qquad \text{(model } 2d-2\text{)}. \tag{28}$$

The results of the regression are given in table 3. Again, the least-squares error was tracked as a function of $n_{\min}$. The regressions only became statistically acceptable at the 95% level for $n_{\min} = 40$, and good fits were obtained for $n_{\min} = 50$ and higher. By taking the results at $n_{\min} = 50$ as our best estimates, we get

$$\mu = 2.638\,07 \pm 0.000\,12 \tag{29}$$

with a 67% statistical confidence interval. This demonstrates that the statistic (a_+/a_-) can also be tracked and analysed to obtain estimates for μ.

There are no *a priori* reasons to accept any one of the above results as our best estimate, so we averaged them and took the largest confidence interval as an error bar:

$$\mu = 2.638\,05 \pm 0.000\,12. \tag{30}$$

This result is consistent with the estimates in equations (7), (9), (15) and (16).

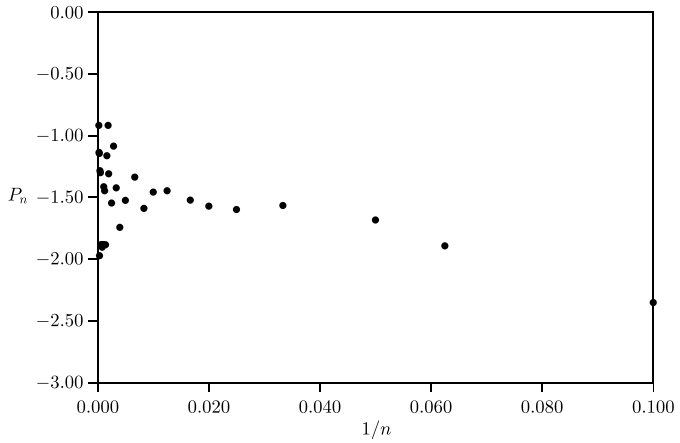

Figure 5. Scatterplot of $P_n = n(\log(\frac{\langle a_+\rangle}{\langle a_-\rangle}) - \log\mu^2)/2$ against $1/n$. Error bars have been left away for clarity. μ^2 was set equal to its least-squares value in equation (30). The data points accumulate around -1.5; this is consistent with $\alpha = 1/2$.

Table 3. Least-squares analysis results: model $2d - 2$.

$n_{\min}$	$\log\mu^2$	a_2	χ^2(d f)	Level
10	$1.938\,531 \pm 0.000\,072$	4.286 ± 0.018	1454(26)	100%
16	$1.938\,146 \pm 0.000\,076$	4.582 ± 0.025	1307(25)	100%
20	$1.938\,544 \pm 0.000\,077$	4.242 ± 0.029	1012(24)	100%
30	$1.939\,493 \pm 0.000\,081$	3.375 ± 0.037	236(23)	100%
40	$1.939\,925 \pm 0.000\,084$	2.951 ± 0.043	56.4(22)	100%
50	$1.940\,094 \pm 0.000\,087$	2.775 ± 0.049	27.3(21)	83.9%
60	$1.940\,138 \pm 0.000\,090$	2.726 ± 0.055	25.5(20)	81.8%
80	$1.940\,137 \pm 0.000\,095$	2.727 ± 0.065	25.5(19)	85.6%

The exponent α in equation (5) can also be estimated from our data. By equation (26) we observe that

$$\left(\log\left(\frac{\langle a_+\rangle_n}{\langle a_-\rangle_n}\right) - \log\mu^2\right) = a_2\log((n+2)/n)) + O(1/n), \tag{31}$$

and hence by approximating $\log((n+2)/n) \approx 2/n$ and plotting $P_n = n\big(\log\big(\frac{\langle a_+\rangle_n}{\langle a_-\rangle_n}\big) - \log\mu^2\big)\big/2$ against $1/n$, the Y-intercept should be $a_2 = \alpha - 2$ as $1/n \to 0^+$. These data are plotted in figure 5 as a scatter plot for clarity. The data points accumulate close to -1.5; this is consistent with the expectation that $\alpha = 1/2$ in this model. A weighted least-squares fit to the data in figure 5 using the model

$$\frac{n}{2}\left(\log\left(\frac{\langle a_+\rangle}{\langle a_+\rangle}\right) - \log\mu^2\right) = (\alpha - 2) + \frac{a1}{n} + \frac{a2}{n^2} \tag{32}$$

gives a statistically acceptable regression at the 78% level. The estimate for the specific heat exponent is $2 - \alpha = -1.468 \pm 0.027$ with a 67% confidence interval. Thus, we estimate $\alpha = 0.532 \pm 0.027$. Hyperscaling in models of self-avoiding walks is exhibited in the scaling relation $2 - \alpha = 1/\phi = \mathrm{d}\nu$ in d dimensions, where ν is the metric exponent and ϕ is the crossover exponent. Conformal field theory and Coulomb gas techniques show that the exact value for the metric exponent is $\nu = 3/4$, and thus $\phi = 2/3$ and $\alpha = 1/2$ by hyperscaling

Table 4. Atmospheres in three dimensions. The estimates for $\langle a_+/a_-\rangle_n$ are modified by putting $a_- = 1$ whenever the negative atmosphere of a polygon is empty. In addition, observe that these raw data give two times $\langle a_+\rangle_n$ and $\langle a_-\rangle_n$.

n	$\langle a_+/a_-\rangle$	$2\langle a_+\rangle$	$2\langle a_-\rangle$	Ratio
10	15.7918 ± 0.0171	45.4003 ± 0.0146	3.2247 ± 0.0046	14.079 ± 0.025
16	21.476 ± 0.028	70.117 ± 0.023	4.0795 ± 0.0055	17.188 ± 0.029
20	23.512 ± 0.038	87.117 ± 0.031	4.7959 ± 0.0069	18.165 ± 0.033
30	25.370 ± 0.044	130.611 ± 0.040	6.7335 ± 0.0085	19.397 ± 0.031
40	25.339 ± 0.042	174.729 ± 0.048	8.7046 ± 0.0096	20.073 ± 0.028
50	24.723 ± 0.039	219.059 ± 0.055	10.7366 ± 0.0110	20.403 ± 0.027
60	24.224 ± 0.035	263.598 ± 0.059	12.7390 ± 0.0120	20.692 ± 0.025
80	23.458 ± 0.028	352.742 ± 0.069	16.8055 ± 0.0142	20.990 ± 0.022
100	23.077 ± 0.024	442.079 ± 0.079	20.8720 ± 0.0163	21.180 ± 0.021
120	22.862 ± 0.021	531.484 ± 0.089	24.9350 ± 0.0184	21.315 ± 0.020
150	22.6420 ± 0.0184	665.734 ± 0.096	31.049 ± 0.021	21.4414 ± 0.0176
200	22.4215 ± 0.0163	889.395 ± 0.116	41.285 ± 0.026	21.5428 ± 0.0164
250	22.3361 ± 0.0144	1113.621 ± 0.134	51.457 ± 0.028	21.6418 ± 0.0143
300	22.2695 ± 0.0138	1337.490 ± 0.153	61.650 ± 0.032	21.6949 ± 0.0138
350	22.2022 ± 0.0125	1561.350 ± 0.167	71.914 ± 0.035	21.7113 ± 0.0129
400	22.1758 ± 0.0118	1785.610 ± 0.181	82.100 ± 0.037	21.7492 ± 0.0121
500	22.1269 ± 0.0105	2233.66 ± 0.21	102.529 ± 0.042	21.7856 ± 0.0110
600	22.0821 ± 0.0099	2682.08 ± 0.23	123.025 ± 0.048	21.8011 ± 0.0104
700	22.0839 ± 0.0093	3130.35 ± 0.25	143.325 ± 0.053	21.8409 ± 0.0099
800	22.0469 ± 0.0090	3578.04 ± 0.28	163.868 ± 0.058	21.8349 ± 0.0095
900	22.0442 ± 0.0088	4026.85 ± 0.31	184.236 ± 0.064	21.8570 ± 0.0093
1000	22.0312 ± 0.0066	4474.69 ± 0.26	204.668 ± 0.053	21.8632 ± 0.0070
1200	22.0170 ± 0.0062	5371.08 ± 0.30	245.510 ± 0.060	21.8772 ± 0.0066
1500	21.9997 ± 0.0056	6715.97 ± 0.33	306.839 ± 0.068	21.8876 ± 0.0060
2000	21.9897 ± 0.0050	8957.19 ± 0.39	408.922 ± 0.081	21.9044 ± 0.0053
2500	21.9753 ± 0.0040	11198.70 ± 0.39	511.163 ± 0.080	21.9083 ± 0.0042
3000	21.9696 ± 0.0037	13439.49 ± 0.44	613.286 ± 0.091	21.9139 ± 0.0040
3500	21.9627 ± 0.0036	15680.75 ± 0.48	715.523 ± 0.101	21.9151 ± 0.0038
4000	21.9652 ± 0.0033	17923.15 ± 0.52	817.535 ± 0.111	21.9234 ± 0.0037
5000	21.9545 ± 0.0031	22404.56 ± 0.59	1022.050 ± 0.125	21.9212 ± 0.0033

[35, 36]. These values are consistent with the numerical estimate of α above, which includes $1/2$ within its 95% confidence interval.

3.2. Results in three dimensions

We performed similar simulations and calculations in three dimensions. The data collected in three dimensions are displayed in table 4.

The model

$$\log\left(\frac{\langle a_+\rangle_n}{\langle a_-\rangle_n}\right) = \log\mu^2 + a_2\log((n+2)/n)) + a_3/n^2, \qquad \text{(model } 3d-1\text{)} \qquad (33)$$

was examined for the ratios of the atmospheric data in table 4. Regression data for this model are listed in table 5. Even for $n_{\min} = 10$ the regression is acceptable at the 95% level on 26 degrees of freedom. In this case, the best estimate obtained for μ is $\mu = 4.683\,644 \pm 0.000\,037$. Increasing the value of $n_{\min}$ to 20 gave $4.683\,867 \pm 0.000\,038$, which is outside the error bar at

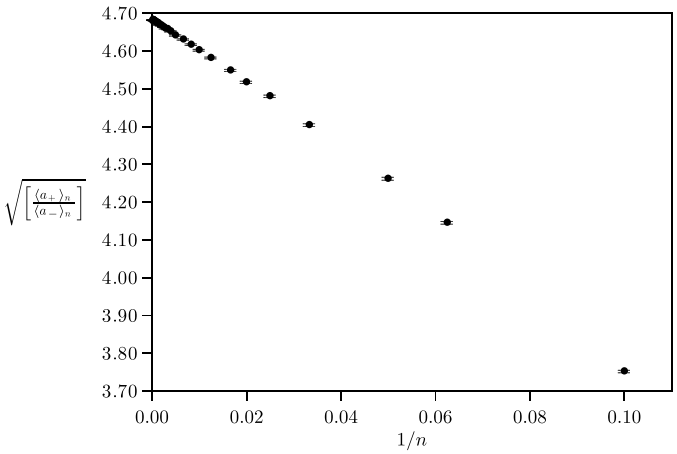

Figure 6. The ratio $[\langle a_+\rangle_n/\langle a_-\rangle_n]^{1/2}$ plotted against $1/n$ in the cubic lattice. Extrapolation of the data to infinite n is done by a regression with the model $3d-1$ to estimate μ.

Table 5. Least-squares analysis results: model $3d-1$.

$n_{\min}$	$\log \mu^2$	a_2	χ^2(d f)	Level
10	$3.088\,153 \pm 0.000\,048$	-1.654 ± 0.0192	33.4(26)	85%
16	$3.088\,237 \pm 0.000\,049$	-1.714 ± 0.0136	11.3(25)	0.8%
20	$3.088\,248 \pm 0.000\,050$	-1.723 ± 0.0158	10.7(24)	0.9%
30	$3.088\,244 \pm 0.000\,053$	-1.720 ± 0.021	10.7(23)	1.4%
40	$3.088\,263 \pm 0.000\,055$	-1.737 ± 0.025	9.9(22)	1.2%

$n_{\min} = 10$. Further increases in $n_{\min}$ did not cause further significant changes in the estimate, and we take the value at $n_{\min} = 20$ to be our best estimate,

$$\mu = 4.683\,867 \pm 0.000\,038. \tag{34}$$

The model

$$\log\left\langle \frac{a_+}{a_-}\right\rangle_n = \log\mu^2 + a_2 \log\left((n+2)/n\right)) + a_3/n^2, \qquad \text{(model } 3d-2\text{)} \tag{35}$$

was also examined. Regression data is given in table 6. The fits were not acceptable for small values of $n_{\min}$, but the quality of the regressions increased with increasing $n_{\min}$ and regressions acceptable at the 95% level were obtained for $n_{\min} \geqslant 50$. In this case the best estimate obtained for μ is

$$\mu = 4.683\,972 \pm 0.000\,041. \tag{36}$$

Further increases in $n_{\min}$ to 60 gave $4.684\,092 \pm 0.000\,042$, which is outside the error bar at $n_{\min} = 50$. Further increases in $n_{\min}$ did not cause further significant changes in this estimate, and we took the value at $n_{\min} = 60$ to be our best estimate:

$$\mu = 4.684\,092 \pm 0.000\,042. \tag{37}$$

There are no *a priori* reasons to accept any one of the above results as our best estimate, so we averaged them and took the largest confidence interval as an error bar: $\mu = 4.683\,980 \pm 0.000\,042$. There is an unknown systematic error due to deficiencies in

Table 6. Least-squares analysis results: model $3d-2$.

$n_{\min}$	$\log \mu^2$	a_2	$\chi^2(\mathrm{d}\ f)$	Level
10	$3.087\,069 \pm 0.000\,044$	3.2151 ± 0.0099	3459(26)	100%
16	$3.086\,527 \pm 0.000\,046$	3.6196 ± 0.0142	2678(25)	100%
20	$3.086\,816 \pm 0.000\,047$	3.3815 ± 0.0163	2239(24)	100%
30	$3.087\,665 \pm 0.000\,050$	2.631 ± 0.022	640(23)	100%
40	$3.088\,140 \pm 0.000\,052$	2.176 ± 0.026	80.5(22)	100%
50	$3.088\,293 \pm 0.000\,054$	2.019 ± 0.029	18.3(21)	36.7%
60	$3.088\,344 \pm 0.000\,055$	1.964 ± 0.033	11.8(20)	7.6%
80	$3.088\,317 \pm 0.000\,059$	1.994 ± 0.039	10.8(20)	6.8%

our models. If we take one-half of the absolute distance between the two estimates, then the systematic error may be estimated as 0.000 067. Thus, we take as our best estimate

$$\mu = 4.683\,980 \pm 0.000\,042 \pm 0.000\,067, \tag{38}$$

the result in equation (38), where we add a systematic error of size 0.000 067 to the confidence interval. This result compares well with the estimate by Clisby, Liang and Slade [5] in equation (11).

The corrections to the powerlaw and exponential growth in equation (5) are more explicitly thought to be of the form

$$p_n = An^{\alpha-2}\mu^n(1 + Bn^{-\Delta} + o(n^{-\Delta})), \tag{39}$$

where Δ is the *confluent exponent* and B is a constant (see, for example, [32]). In two dimensions the value of Δ is numerically close to 1, thus the least-squares analysis for the two-dimensional data in table 1 would not be influenced by the presence of such a confluent term. This is not necessary the case in three dimensions, where $\Delta \approx 1/2$.

To investigate the effects of a confluent correction on our best estimate in equation (38), we repeated our analysis with a confluent term present by using the models

$$\log\left(\frac{\langle a_+\rangle_n}{\langle a_-\rangle_n}\right) = \log\mu^2 + a_2/\sqrt{n} + a_3/n, \qquad (\text{model } 3d-3) \tag{40}$$

and

$$\log\left\langle\frac{a_+}{a_-}\right\rangle_n = \log\mu^2 + a_2/\sqrt{n} + a_3/n, \qquad (\text{model } 3d-4). \tag{41}$$

The results of the regressions are given in tables 7 and 8, respectively.

The regression data in table 7 indicate that our numerical data were described well by this model $3d-3$ in equation (40) with the inclusion of a confluent correction term. The fits are acceptable starting at $n_{\min} = 20$, but there is still a drift in the result with increasing $n_{\min}$. For values of $n_{\min} \geqslant 50$ we obtain estimates of the parameters which do not exclude previous estimates outside their error bars; at $n_{\min} = 50\mu = 4.683\,574 \pm 0.000\,104$ and at $n_{\min} = 100$, $\mu = 4.683\,82 \pm 0.000\,14$. At $n = 120$ the result is $\mu = 4.683\,89 \pm 0.000\,16$. This result is included in the confidence interval of our best estimate in equation (38), and we conclude that the results in this model is consistent with those obtained from models $3d-1$ and $3d-2$. The confluent correction did not influence our statistical estimate in a systematic way which would be visible outside the confidence intervals stated above.

We also examined our the data collected for $\langle a_+/a_-\rangle_n$ using model $3d-4$ with a confluent term. The results are given in table 8. Observe that the regressions were not good until $n_{\min} = 80$ and that there is only a slow improvement for values of $n_{\min} \geqslant 100$. While

Table 7. Least-squares analysis results: model $3d-3$.

$n_{\min}$	$\log \mu^2$	a_2	$\chi^2(\mathrm{d}\ f)$	Level
16	$3.087\,493 \pm 0.000\,107$	0.0494 ± 0.0049	44.9(25)	99.2%
20	$3.087\,780 \pm 0.000\,115$	0.0314 ± 0.0056	21.5(24)	38.2%
30	$3.087\,986 \pm 0.000\,127$	0.0191 ± 0.0065	14.0(23)	7.3%
40	$3.088\,123 \pm 0.000\,136$	0.0102 ± 0.0072	10.1(22)	1.4%
50	$3.088\,110 \pm 0.000\,145$	0.0111 ± 0.0080	10.1(21)	2.1%
60	$3.088\,209 \pm 0.000\,154$	0.0042 ± 0.0088	8.4(20)	1.1%
80	$3.088\,198 \pm 0.000\,169$	0.0050 ± 0.0100	8.4(19)	1.7%
100	$3.088\,230 \pm 0.000\,183$	0.0026 ± 0.0113	8.3(18)	2.5%
120	$3.088\,26 \pm 0.000\,20$	0.0004 ± 0.0129	8.1(17)	3.7%

Table 8. Least-squares analysis results: model $3d-4$.

$n_{\min}$	$\log \mu^2$	a_2	$\chi^2(\mathrm{d}\ f)$	Level
60	$3.090\,090 \pm 0.000\,150$	-0.1434 ± 0.0087	78.0(20)	100%
80	$3.089\,504 \pm 0.000\,161$	-0.1012 ± 0.0098	33.0(19)	97.6%
100	$3.089\,207 \pm 0.000\,174$	-0.0791 ± 0.0109	22.3(18)	78.1%
120	$3.089\,012 \pm 0.000\,188$	-0.0641 ± 0.0122	18.6(17)	64.5%
150	$3.088\,71 \pm 0.000\,21$	-0.0408 ± 0.0141	13.3(16)	34.2%
200	$3.088\,40 \pm 0.000\,22$	-0.0157 ± 0.0169	9.6(15)	15.5%
250	$3.088\,46 \pm 0.000\,27$	-0.020 ± 0.020	9.5(14)	20.1%
300	$3.088\,31 \pm 0.000\,30$	-0.007 ± 0.023	8.9(13)	21.4%

fits became statistically acceptable at $n_{\min} = 100$, there remained a persistent downwards drift in the estimate of $\log \mu^2$. These estimates appear to stabilize around $n_{\min} = 200$, which is included in the confidence interval at $n_{\min} \geqslant 250$. If $n_{\min} = 300$, then obtain $\mu = 4.684\,01 \pm 0.000\,23$, which is included in the confidence intervals of our best estimate in equation (38). Thus, we again conclude that ignoring the confluent correction in model $3d-2$ did not affect our statistical estimate in a systematic way which would be visible outside the statistical confidence intervals stated.

As was the case in two dimensions, our data are consistent with the exponent α in equation (5). By plotting $P_n = n\big(\log\big(\frac{\langle a_+\rangle_n}{\langle a_-\rangle_n}\big) - \log\mu^2\big)\big/2$ against $1/n$, and by considering equation (33), it follows that the Y-intercept should be at $a_2 = \alpha - 2$ as $1/n \to 0^+$. The data are plotted in figure 7 as a scatter plot.

The data points accumulate close to -1.75; this is consistent with the expectation that $\alpha \approx 0.25$ in this model. A weighted least-squares fit to the data in figure 5 using the model

$$\frac{n}{2}\left(\log\left(\frac{\langle a_+\rangle}{\langle a_+\rangle}\right) - \log\mu^2\right) = (\alpha - 2) + \frac{a1}{n} + \frac{a2}{n^2} \tag{42}$$

gives a statistically acceptable regression. The estimate for the specific heat exponent is $2 - \alpha = -1.7525 \pm 0.0151$ with a 67% confidence interval. Increasing $n_{\min}$ in the fit did not change this estimate outside its confidence intervals, and so our best estimate is $\alpha = 0.248 \pm 0.016$. These results are consistent with the estimates in [5] where it is estimated that α is in the range 0.23 to 0.24.

Assuming the hyperscaling relation $\mathrm{d}\nu = 2 - \alpha$ and using the value $\nu = 0.5874 \pm 0.0002$ estimated by Prellberg [41] shows that $\alpha = 0.2378 \pm 0.0006$ if hyperscaling applies in this

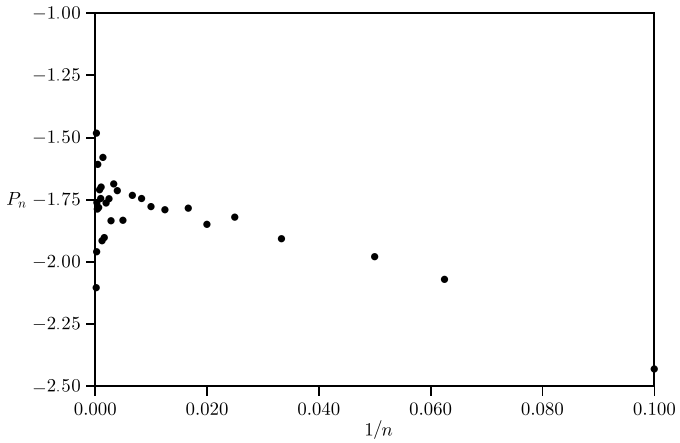

Figure 7. Scatterplot of $P_n = n(\frac{\langle a_+\rangle}{\langle a_-\rangle} - \log\mu^2)/2$ against $1/n$. Error bars have been removed for clarity. μ^2 was set equal to its least-squares value in equation (38). The data points accumulate around -1.77; this is consistent with $\alpha \approx 0.23$.

model. This value of α is inside the confidence interval of our estimate for α, and our result is consistent with hyperscaling in three-dimensional polygons.

4. Relative free energy of knotted polygons

In this section, we turn our attention to polygons in the cubic lattice with fixed knot type. Knotted polygons have received attention in the literature [33, 34, 40, 44] as models of knotted polymers.

We define $p_n(K)$ to be the number of lattice polygons of length n and with knot type K, (counted up to translations in the lattice). The atmospheres of a polygon of fixed knot type are defined as in section 2, and following the arguments leading up to equation (23), it follows that

$$\frac{p_{n+2}(K)}{p_n(K)} = \frac{\langle a_+(K)\rangle_n}{\langle a_-(K)\rangle_{n+2}}. \tag{43}$$

Observe that the knot type of the polygon is not changed by adding edges around positive atmospheric squares, or by removing edges around negative atmospheric squares.

There is little known about $p_n(K)$. In particular, it is normally assumed that

$$p_n(K) \approx C_K n^{(\alpha_K - 2)}(\mu_K)^n, \tag{44}$$

where μ_K is a growth constant, α_K is an entropic exponent of polygons of knot type K and C_K is a constant. Simulations indicate that $\alpha_K = \alpha_\emptyset + N_K$ where N_K is the number of prime components in the knot K and that $\alpha_\emptyset = \alpha$, where $\alpha_\emptyset$ is the entropic exponent of unknotted polygons, and $\alpha \approx 0.25$ is the entropic exponent of polygons in the cubic lattice [39].

We define the entropy of polygons of length n and knot type K by

$$E_n(K) = \log p_n(K) \tag{45}$$

and the relative entropy is then given from equation (43) by

$$E_{n+2}(K) - E_n(K) = \log\langle a_+(K)\rangle_n - \log\langle a_-(K)\rangle_{n+2}. \tag{46}$$

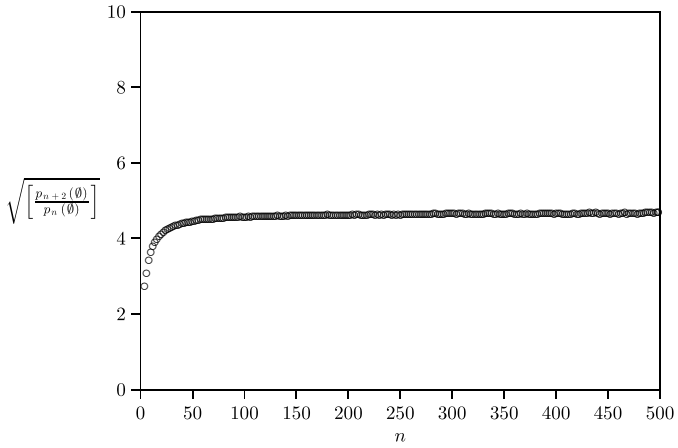

Figure 8. The ratio $[p_{n+2}(\emptyset)/p_n(\emptyset)]^{1/2}$ against n for unknotted polygons. Note that the data appear to be monotonically increasing to a limiting value.

Kesten's pattern theorem for polygons (see [44]) suggests that $\langle a_+(K)\rangle_n/n \to \alpha_+$ and $\langle a_-(K)\rangle_n/ \to \alpha_-$ as $n \to \infty$, where α_+ and α_- are constants. Taking n to infinity in the last equation shows that

$$\lim_{n\to\infty} (E_{n+2}(K) - E_n(K)) = \log(\alpha_+/\alpha_-). \tag{47}$$

In other words, a plot of $[p_{n+2}(K)/p_n(K)]^{1/2}$ against n will approach the ratio $(\alpha_+/\alpha_-)^{1/2}$. Such a plot is given in figure 8 for $K = \emptyset$, the unknot.

The entropy of knotted polygons of knot type K is given by

$$E_n(K) = \sum_{m=n_{\min}}^{n-2} (E_{m+2}(K) - E_m(K)) + E_{n_{\min}}(K), \tag{48}$$

where $n_{\min}$ is the minimum number of edges necessary to realize a polygon of knot type K in the cubic lattice [7, 19] (this is the *minimal edge number* of the knot type). This shows that

$$E_n(K) = \sum_{m=n_{\min}}^{n-2} \left[\log\left(\frac{\langle a_+(K)\rangle_n}{\langle a_-(K)\rangle_{n+2}}\right)\right] + E_{n_{\min}}(K). \tag{49}$$

The absolute entropy of knotted polygons for $n = n_{\min}$ is an issue which have been addressed for polygons of knot type 3_1 (trefoils) by Diao [8]. In this case, $p_{24}(3_1) = 3496$ since $n_{\min} = 24$ for trefoils, and thus the entropy is $E_{24}(3_1) = \log 3496$. By computing the area under the curve $\log(\langle a_+(K)\rangle_n/\langle a_-(K)\rangle_{n+2})$ and adding the entropy at $n_{\min}$, the entropy of knotted polygons at larger values of n can be determined. We did not follow this approach, but instead focused on determining the relative entropies of knotted polygons.

Unknotted polygons were sampled in the grand canonical ensemble by using the BFACF algorithm [1, 2] which is known to be ergodic for polygons of fixed knot types in the cubic lattice [18, 21]. Polygons of fixed knot type K were sampled along a Markov Chain for 2×10^9 iterations with data collected every 200 iterations for a time-series of length 10^7 of positive and negative atmospheres.

The data along the time series were binned according to length, and then were analysed at each fixed length to estimate $\langle a_+(K)\rangle_n$ and $\langle a_-(K)\rangle_n$. Throughout the simulations, the parameter of the BFACF algorithm was set close to its critical value to obtain enough data at

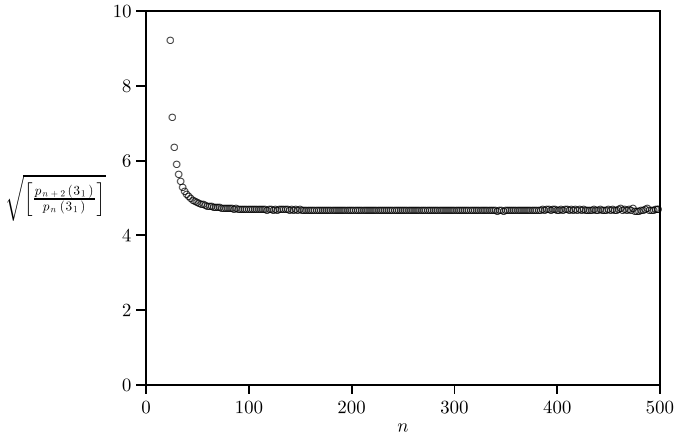

Figure 9. The ratio $[p_{n+2}(3_1)/p_n(3_1)]^{1/2}$ against n for polygons with knot type the trefoil. In contrast with the data in figure 8, the statistic appears to be monotonically decreasing with n. Observe that $n \geqslant 24$, since the polygons with knot type 3_1 have length at least 24 edges.

large values of n (up to $n = 500$). These calculations did not produce uncorrelated data at neighbouring values of n, but statistical error bars at any given value of n were small, and plots of the data show reasonably smooth curves.

In the case of unknotted polygons (see figure 8) it is known that the limit

$$\mu_\emptyset = \lim_{n\to\infty} [p_n(\emptyset)]^{1/n} \tag{50}$$

exists via a concatenation argument [44]. Thus, one may expect that

$$\lim_{n\to\infty} \left[\frac{p_{n+2}(\emptyset)}{p_n(\emptyset)}\right] = \mu_\emptyset^2. \tag{51}$$

This remains an open question, even though figure 8 provides strong evidence in its favour. While the data in figure 8 quickly settles down close to $\mu_\emptyset$ for (say) $n > 50$, it is an increasing curve indicating that relative entropy (equation (46) increases steeply with n for small values of n.

In figure 9 data for the trefoil knot is plotted. The limit

$$\mu_{3_1} = \limsup_{n\to\infty} [p_n(3_1)]^{1/n} \tag{52}$$

is not known to exist, but we give strong numerical data in figure 9 that

$$\limsup_{n\to\infty} \left[\frac{p_{n+2}(3_1)}{p_n(3_1)}\right] = \mu_{3_1}^2 \tag{53}$$

exists as a limit. In addition, the data suggest that any difference in the values of $\mu_\emptyset$ and μ_{3_1} will be small. This is consistent with previous data suggesting that $\mu_\emptyset = \mu_{3_1}$ [39]. Figure 9 also show that the relative entropy of polygons with knot type 3_1 decreases with increasing n. This is opposite to behaviour for the unknot in figure 8, and it seems likely that the limit (53) approaches $\mu_{3_1}^2$ from above, while the limit (51) approaches $\mu_\emptyset^2$ from below.

In figure 10, curves are plotted for the unknot and for compounded trefoils against n. The starting points of the curves increases with the number of knot components in each knotted polygon, since the number of edges required to realize the knots, $n_{\min}$, increases with the number of components. The data are plotted for the unknot ($\emptyset$), the trefoil (3_1), the square knot $\left(3_1^+\#3_1^-\right)$, the granny knot $\left(3_1^+\#3_1^+\right)$ and a compound knot with three trefoil components of

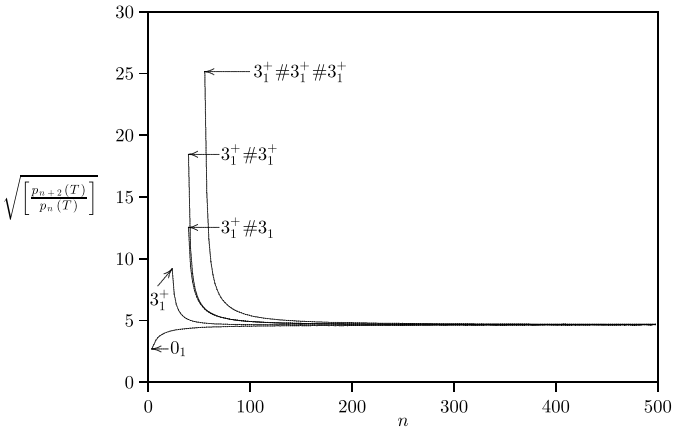

Figure 10. The ratio $[p_{n+2}(T)/p_n(T)]^{1/2}$ against n for polygons with knot types the unknot ($\emptyset$), trefoil (3_1), the square knot ($3_1^+\#3_1^-$), the granny knot ($3_1^+\#3_1^+$) and a compound knot with three trefoil components of the same chirality ($3_1^+\#3_1^+\#3_1^+$). Observe the marked difference at small n between the granny and square knots—the granny knot has much more relative entropy than the square knot at low values of n.

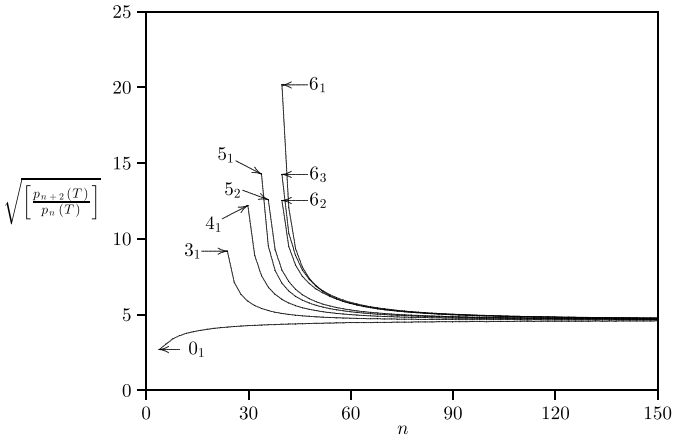

Figure 11. The ratio $[p_{n+2}(T)/p_n(T)]^{1/2}$ against n for polygons of six crossing knot types. The most relative entropy is found in 6_1 and the least in the square knot and 6_2, for small values of n. Observe that the square knot and 6_2 has virtually the same change in relative entropy with increasing n.

the same chirality $\left(3_1^+\#3_1^+\#3_1^+\right)$. Observe the marked difference at small n between the granny and square knots. The granny knot has much more relative entropy than the square knot at low values of n.

In figures 11 and 12 data are given for a collection of prime knots. The data in figure 12 are for prime knots to six crossings, for $n \in [0, 150]$, while these data are also included in figure 11 for a larger collection of prime knots, for $n \in [0, 75]$. The larger scale on the X-axis improves the resolution of the data in these graphs.

It is noticeable that the ratios approach (within numerical precision) the same limiting curve with increasing n in these graphs. More interesting are the differences between different knot types for small values of n—there are marked and persistent differences between knots with the same minimal crossing numbers (for example 5_1 and 5_2), and the ratio $p_{n+2}(K)/p_n(K)$

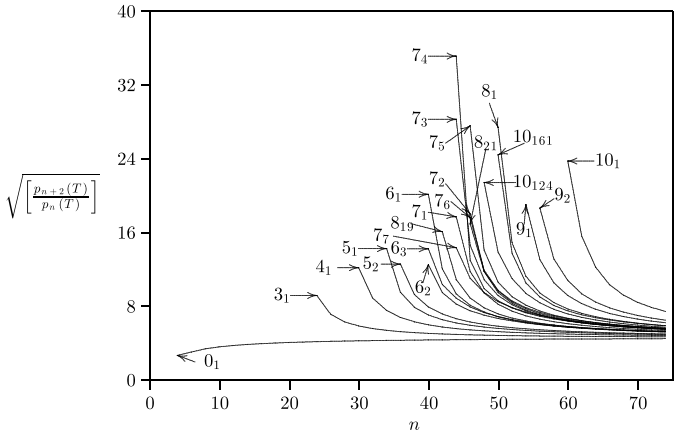

Figure 12. The ratio $[p_{n+2}(T)/p_n(T)]^{1/2}$ against n for knotted polygons with crossing number up to ten crossing knot types. Relative entropy at small values of n is large for 7_4, 8_1 and 7_3, amongst these knot types.

can differ by factors of as large as four or five for different knot types. Most remarkable though there are individual differences between different knot types; each knot type appears to have its own characteristic profile in these graphs, and some (such as 7_4) presents anomalously large ratios close to its minimal edge number.

5. Conclusions

In this paper, we presented a numerical method for the calculation of relative entropies of polygons. The method is implemented by defining two statistics (the positive and negative atmospheres) of a polygon. By calculating these statistics, one may determine ratios of the form p_{n+2}/p_n in models of polygons, and we have done this in order to estimate the growth constants. For knotted polygons, we are able to determine the relative differences in the entropy as a function of the knot types.

This technique is quite general, and can be used on other lattice models, for example lattice walks, trees or animals. In addition, it can also be used to estimate free energies in interacting models of lattice polygons, for example adsorbing polygons or collapsing polygons. We show this in the appendix.

In section 3, we estimated the growth constants of polygons in the square and cubic lattices. We determine $\mu = 2.638\,05 \pm 0.000\,11$ in the square lattice, and $\mu = 4.683\,980 \pm 0.000\,042 \pm 0.000\,067$ in the cubic lattice. These estimates compare well with estimates by other means in equations (7) and (9) in the square lattice, and equation (11) in the cubic lattice. While our results are not as accurate in the square lattice, where series analysis of polygon and self-avoiding walk data gave μ to very high accuracy, our result is an independent confirmation of the first digits in those estimates.

In three dimensions our cubic lattice estimate is comparable in accuracy to the recent estimate by Clisby, Liang and Slade [5] in equation (11). We confirm their estimate to four decimal places. We believe that the methods here can be used to find μ to even higher accuracy in the cubic lattice by using more computer resources.

In section 4, we considered the relative entropies of polygons of fixed knot types. Little is known about such polygons, but our numerical data show that limits such as in

equations (51) and (53) exists. In addition, we plotted those ratios in figures 9–12, and in each case found that the relative entropy of an unknotted polygon increasing with increasing n, while it decreases for a knotted polygon with increasing n. In each case it approaches a constant. We also observe that different knots have very different relative entropies at small values of n as in figure 12. This shows that for small values of n these knots will have different statistical properties, a fact which may influence the physical properties of short knotted polymer rings.

Acknowledgments

EJJvR and AR acknowledge support in the form of Discovery Grants from NSERC (Canada). We are grateful to a referee who contributed to the derivation in the appendix.

Appendix. Atmospheres of interacting polygons

It is possible to generalize atmospheres to models of polygons weighted by a Boltzmann factor β. Such models are *interacting*, and typically have a partition function

$$Z_n(\beta) = \sum_m p_n(m)\beta^m = \sum_\omega \beta^{m(\omega)}, \tag{A.1}$$

where $p_n(m)$ is the number of polygons of length n counted up to translational invariance, and with *energy* m (the number of contacts, visits, span, or the number of occurrences of any other property). The second sum is over all polygons ω of length n and with energy $m(\omega)$.

In models such as these the construction in figure 1 changes both the length and the energy of a polygon. Consider a polygon ω of length n and energy $m(\omega)$. Similarly, let ν be a polygon of length $n+2$ and energy $m(\nu)$. These polygons may be associated with an atmospheric square as in figure 1; in particular, ω may have a positive atmospheric square which produces ν (in which case there is a negative atmospheric square in ν which produces ω). This association is indicated schematically by edges in figure 3, and we call ω and ν *linked* by an atmospheric move.

We now assign a weight $W(\omega \to \nu)$ to the edges in figure 3. At this point, we propose to define these weights by

$$W(\omega \to \nu) = \begin{cases} \min\{1, \beta^{m(\nu)-m(\omega)}\}, & \text{if} \quad \omega \text{ and } \nu \text{ are linked,} \\ 0, & \text{otherwise,} \end{cases} \tag{A.2}$$

but we shall later see that this definition is somewhat arbitrary. Observe that if $W(\omega \to \nu) = \beta^{m(\nu)-m(\omega)} \leqslant 1$, then $W(\nu \to \omega) = 1$ and vice versa. In fact, the weights satisfy

$$W(\omega \to \nu) = W(\nu \to \omega)\beta^{m(\nu)-m(\omega)} \tag{A.3}$$

for all possible pairs of walks (ω, ν) (with the length of ω equal to n and the length of ν equal to $n+2$).

Multiply this last equation by $\beta^{m(\omega)}$ and sum both sides over ω and ν; this gives

$$\sum_\omega \left(\sum_\nu W(\omega \to \nu) \right) \beta^{m(\omega)} = \sum_\nu \left(\sum_\omega W(\nu \to \omega) \right) \beta^{m(\nu)}, \tag{A.4}$$

where we keep in mind that $W(\omega \to \nu) = 0$ if ω and ν and not linked.

Next define the positive atmosphere of a polygon ω of length n by

$$\alpha_+(\omega) = \sum_{\nu} W(\omega \to \nu), \tag{A.5}$$

where the sum is over polygons of length $n+2$ which are linked to ω. Similarly, define the negative atmosphere of a polygon of length $n+2$ by

$$\alpha_-(\nu) = \sum_{\omega} W(\nu \to \omega), \tag{A.6}$$

where the sum is over all polygons of length n which are linked to ν. Then equation (A.4) becomes

$$\sum_{\omega} \alpha_+(\omega)\beta^{m(\omega)} = \sum_{\nu} \alpha_-(\nu)\beta^{m(\nu)}, \tag{A.7}$$

where we keep in mind that the sum over ω is over polygons of length n and the sum over ν is over polygons of length $n+2$. Dividing the last equation by $Z_n(\beta)$ and noting that the weighted means of the atmospheres are given by

$$\langle\alpha_+\rangle_n = \frac{\sum_\omega \alpha_+(\omega)\beta^{m(\omega)}}{Z_n(\beta)}, \qquad \langle\alpha_-\rangle_{n+2} = \frac{\sum_\nu \alpha_-(\nu)\beta^{m(\nu)}}{Z_{n+2}(\beta)},$$

then finally produces the result

$$\frac{Z_{n+2}(\beta)}{Z_n(\beta)} = \frac{\langle\alpha_+\rangle_n}{\langle\alpha_-\rangle_{n+2}} \approx \frac{\langle\alpha_+\rangle_n}{\langle\alpha_-\rangle_n}, \tag{A.8}$$

where one expects the approximation to become more accurate with increasing n.

Implementing the above involves the sampling of polygons from a Boltzman distribution

$$D_n(\omega) = \frac{\beta^{m(\omega)}}{Z_n(\beta)} \tag{A.9}$$

on polygons of length n along a Markov chain, say $\{\omega_i\}_{i=1}^N$ (where $m(\omega)$ is the energy of ω). Then one may estimate $\langle\alpha_+\rangle_n$ by forming the average

$$\langle\alpha_+\rangle_n \approx \frac{1}{N}\sum_{i=1}^{N} A_+(\omega_i), \tag{A.10}$$

with the positive atmosphere of ω_i has $N_+(\omega_i)$ unit squares and

$$A_+(\omega_i) = \sum_{j=1}^{N_+(\omega_i)} W(\omega_i \to \nu_{ij}) \tag{A.11}$$

where ν_{ij} is the polygon of length $n+2$ obtained if the jth atmospheric square is added to make a polygon of length $n+2$. A similar definition can be used to define the average negative atmosphere $\langle\alpha_-\rangle_n$.

Finally, we observe that if $\beta = 1$ in equation (A.2), then the above reproduces the atmospheres for unweighted polygons as defined in section 2. Moreover, it appears that the definition of $W(\omega \to \nu)$ is somewhat arbitrary, any function can be used as long as it satisfies the condition in equation (A.3). This, for example, implies that one may use alternative definitions for the atmospheres of a polygon, and still estimate ratios of partition functions. It is unclear if there are conditions for optimal choices of W.

References

[1] Aragão de Carvalho C, Caracciolo S and Fröhlich J 1983 Polymers and $g|\phi|^4$-theory in four dimensions *Nucl. Phys.* B **215** 209–48
[2] Berg B and Foester D 1981 Random paths and random surfaces on a digital computer *Phys. Lett.* **106B** 323–6
[3] Berretti A and Sokal A D 1985 New Monte Carlo method for the self-avoiding walk *J. Stat. Phys.* **40** 483–531
[4] Broadbent S R and Hammersley J M 1957 Percolation processes: I. Crystals and mazes *Math. Proc. Camb. Phil. Soc.* **53** 629–41
[5] Clisby N, Liang R and Slade G 2007 Self-avoiding walk enumeration via the lace expansion *J. Phys. A: Math. Theor.* **40** 10973–1017
[6] de Gennes P G 1979 *Scaling Concepts in Polymer Physics* (New York: Cornell University Press)
[7] Diao Y 1993 Minimal knotted polygons on the cubic lattice *J. Knot Theor. Ram.* **2** 413–25
[8] Diao Y 1994 The number of smallest knots on the cubic lattice *J. Stat. Phys.* **74** 1247–54
[9] Flory P J 1955 Statistical thermodynamics of semi-flexible chain molecules *Proc. R. Soc. Lond.* A **234** 60–73
[10] Flory P J 1969 *Statistical Mechanics of Chain Molecules* (New York: Wiley-Interscience)
[11] Grassberger P 1997 Pruned-enriched Rosenbluth method: simulation of θ-polymers of chain length up to 1000 000 *Phys. Rev.* E **56** 3682–93
[12] Guida R and Zinn-Justin J 1998 Critical exponents of the N-vector model *J. Phys. A: Math. Gen.* **31** 8103–21
[13] Guttmann A J and Conway A R 2001 Square lattice self-avoiding walks and polygons *Ann. Comb.* **5** 319–45
[14] Hammersley J M 1960 Limiting properties of numbers of self-avoiding walks *Phys. Rev.* **118** 656
[15] Hammersley J M 1961 The number of polygons on a lattice *Math. Proc. Camb. Phil. Soc.* **57** 516–23
[16] Hammersley J M and Morton K W 1954 Poor man's Monte Carlo *J. R. Stat. Soc.* B **16** 23–38
[17] Hara T, Slade G and Sokal A 1993 New lower bounds on the self-avoiding-walk connective constant *J. Stat. Phys.* **72** 479–517
[18] Janse van Rensburg E J 1992 Ergodicity of the BFACF algorithm in three dimensions *J. Phys. A: Math. Gen.* **25** 1031–42
[19] Janse van Rensburg E J and Promislow S D 1995 Minimal knots in the cubic lattice *J. Knot Theor. Ram.* **4** 115–30
[20] Janse van Rensburg E J and Rechnitzer A 2003 High precision canonical Monte Carlo determination of the connective constant of self-avoiding trees *Phys. Rev.* E **67** 036116-1–9
[21] Janse van Rensburg E J and Whittington S G 1991 The BFACF algorithm and knotted polygons *J Phys. A: Math. Gen.* **24** 5553–67
[22] Janse van Rensburg E J, Whittington S G and Madras N 1990 The pivot algorithm and polygons: results on the FCC lattice *J Phys. A: Math. Gen.* **23** 1589–612
[23] Jensen I 2003 A parallel algorithm for the enumeration of self-avoiding polygons on the square lattice *J. Phys. A: Math. Gen.* **36** 5731–45
[24] Jensen I 2004 Enumeration of self-avoiding walks on the square lattice *J. Phys. A: Math. Gen.* **37** 5503–24
[25] Jensen I and Guttmann A J 1998 Self-avoiding walks, neighbour-avoiding walks and trials on semi-regular lattices *J. Phys. A: Math. Gen.* **31** 8137–45
[26] Jensen I and Guttmann A J 1999 Self-avoiding polygons on the square lattice *J. Phys. A: Math. Gen.* **32** 4867–76
[27] Kesten H 1963 On the number of self-avoiding walks *J. Math. Phys.* **4** 960–9
[28] Kesten H 1964 On the number of self-avoiding walks: II *J. Math. Phys.* **5** 1128–37
[29] Le Guillou J C and Zinn-Justin J 1989 Accurate critical exponents from field theory *J. Phys.* **50** 1365–70
[30] Madras N, Orlitsky A and Shepp L A 1990 Monte Carlo generation of self-avoiding walks with fixed endpoints and fixed length *J. Stat. Phys.* **58** 159–83
[31] Madras N and Sokal A D 1988 The pivot algorithm: a highly efficient Monte Carlo method for the self-avoiding walk *J. Stat. Phys.* **47** 573–95
[32] Madras N and Slade G 1993 *The Self-Avoiding Walk* (Boston: Birhäuser)
[33] Michels J P J and Wiegel F W 1984 Probability of knots in a polymer ring *Phys. Lett.* **90A** 381–4
[34] Michels J P J and Wiegel F W 1986 On the topology of a polymer ring *Proc. R. Soc. Lond.* A **403** 269–84
[35] Nienhuis B 1982 Exact critical point and critical exponents on $O(n)$ models in two dimensions *Phys. Rev. Lett.* **49** 1062–5
[36] Nienhuis B 1984 Coulomb gas formulation of the two-dimensional phase transitions *Phase Transitions and Critical Phenomena* vol 11 ed C Domb and J L Lebowitz (New York: Academic) pp 1–53
[37] Nidras P 1996 Grand canonical simulations of the interacting self-avoiding walk model *J. Phys. A: Math. Gen.* **29** 7929–42
[38] O'Brien G L 1990 Monotonicity of the number of self-avoiding walks *J. Stat. Phys.* **59** 969–79
[39] Orlandini E, Tesi M C, Janse van Rensburg E J and Whittington S G 1998 Asymptotics of knotted lattice polygons *J. Phys. A: Math. Gen.* **31** 5953–67
[40] Pippenger N 1989 Knots in self-avoiding walks *Disc. Appl. Math.* **25** 273–8

[41] Prellberg T 2001 Scaling of self-avoiding walks and self-avoiding trails in three dimensions *J. Phys. A: Math. Gen.* **34** L599–602
[42] Prellberg T and Owczarek A L 2000 Four-dimensional polymer collapse: pseudo-first-order transition in interacting self-avoiding Walks *Phys. Rev.* E **62** 3780–9
[43] Rechnitzer A and Janse van Rensburg E J 2002 Canonical Monte Carlo determination of the connective constant of self-avoiding walks *J. Phys. A: Math. Gen.* **35** L605–12
[44] Sumners D W and Whittington S G 1988 Knots in self-avoiding walks *J. Phys. A: Math. Gen.* **21** 1689–94